Phys Chem Minerals (2016) 43:503–514
DOI 10.1007/s00269-016-0811-z

ORIGINAL PAPER

A new mineral species ferricoronadite, $Pb[Mn_6^{4+}(Fe^{3+}, Mn^{3+})_2]O_{16}$: mineralogical characterization, crystal chemistry and physical properties

Nikita V. Chukanov[1] · Sergey M. Aksenov[2,3] · Simeon Jančev[4] · Igor V. Pekov[5] · Jörg Göttlicher[6] · Yury S. Polekhovsky[2] · Vyacheslav S. Rusakov[7] · Yuliya V. Nelyubina[3] · Konstantin V. Van[8]

Received: 4 February 2016 / Accepted: 3 April 2016 / Published online: 29 April 2016

Abstract A new mineral ferricoronadite with the simplified formula $Pb(Mn_6^{4+}Fe_2^{3+})O_{16}$ was discovered in the orogenetic zone related to the "Mixed Series" metamorphic complex near the Nežilovo village, Pelagonian massif, Republic of Macedonia. Associated minerals are franklinite, gahnite, hetaerolite, roméite, almeidaite, Mn-analogue of plumboferrite, zincohögbomite analogue with $Fe^{3+} > Al$, zincochromite, Zn-bearing talc, Zn-bearing muscovite, baryte, quartz and zircon. Ferricoronadite is a late hydrothermal mineral forming veinlets up to 8 mm thick in granular aggregate predominantly composed by zinc-dominant spinels. The new mineral is opaque, black, with brownish black streak. The luster is strong submetallic to metallic. The micro-indentation hardness is 819 kg/mm^2. Distinct cleavage is observed on (100). Ferricoronadite is brittle, with uneven fracture. The density calculated from the empirical formula is 5.538 g/cm^3. In reflected light, ferricoronadite is light gray. The reflectance values [R_{max}/R_{min}, % (λ, nm)] are: 28.7/27.8 (470), 27.6/26.6 (546), 27.2/26.1 (589), 26.5/25.5 (650). The IR spectrum shows the absence of H_2O and OH groups. According to the Mössbauer spectrum, all iron is trivalent. The Mn *K*-edge XANES spectroscopy shows that Mn is predominantly tetravalent, with subordinate Mn^{3+}. The chemical composition is (wt%; electron microprobe, Mn apportioned between MnO_2 and Mn_2O_3 based on the charge-balance requirement): BaO 5.16, PbO 24.50, ZnO 0.33, Al_2O_3 0.50, Mn_2O_3 9.90, Fe_2O_3 11.45, TiO_2 4.19, MnO_2 44.81, total 100.84. The empirical formula based on 8 cations Mn + Fe + Ti + Al + Zn *pfu* is $Pb_{1.03}Ba_{0.32}(Mn^{4+}_{4.85}Fe^{3+}_{1.35}Mn^{3+}_{1.18}Ti_{0.49}Al_{0.09}Zn_{0.04})_{\Sigma 8.00}O_{16}$. The crystal structure was determined using single-crystal X-ray diffraction data. The new mineral is tetragonal, space group $I4/m$, $a = 9.9043(7)$, $c = 2.8986(9)$ Å, $V = 284.34(9)$ Å^3, $Z = 1$. In ferricoronadite, double chains of edge-sharing (Mn, Fe, Ti)-centered octahedra are connected via common vertices to form a pseudo-framework with tunnels containing large cations Pb and Ba. The strongest lines of the powder X-ray diffraction pattern [*d*, Å (*I*, %) (*hkl*)] are: 3.497 (33) (220), 3.128 (100) (−130, 130), 2.424 (27) (−121, 121), 2.214 (23) (240, −240), 2.178 (17) (031), 1.850 (15) (141, −141), 1.651 (16) (060), 1.554 (18) (−251, 251). Ferricoronadite is named as an analogue of coronadite $Pb(Mn_6^{4+}Mn_2^{3+})O_{16}$ with the major charge-compensating octahedral cation Fe^{3+} instead of Mn^{3+}.

✉ Nikita V. Chukanov
chukanov@icp.ac.ru

[1] Institute of Problems of Chemical Physics, Russian Academy of Sciences, Chernogolovka, Moscow Region, Russia 142432

[2] Faculty of Geology, St Petersburg State University, University Embankment 7/9, St Petersburg, Russia 199034

[3] Nesmeyanov Institute of Organoelement Compounds, Russian Academy of Sciences, GSP-1, Vavilova St. 28, V-334, Moscow, Russia 119991

[4] Faculty of Technology and Metallurgy, Saints Cyril and Methodius University, Ruger Boskovic 16, 1000 Skopje, Macedonia

[5] Faculty of Geology, Moscow State University, Vorobievy Gory, Moscow, Russia 119991

[6] ANKA Synchrotron Radiation Facility, Karlsruhe Institute of Technology, Hermann-von-Helmholtz-Platz 1, 76344 Eggenstein-Leopoldshafen, Germany

[7] Faculty of Physics, Moscow State University, Vorobievy Gory, Moscow, Russia 119991

[8] Institute of Experimental Mineralogy, Russian Academy of Sciences, Chernogolovka, Moscow Region, Russia 142432

Keywords New mineral · Ferricoronadite · Hollandite supergroup · Crystal structure · Mössbauer spectroscopy · XANES spectroscopy · IR spectroscopy · Reflectance spectrum · Nežilovo · Pelagonian massif

Introduction

The hollandite supergroup includes 2 × 2 tunnel oxides with the simplified general formula $(A^{+}, A^{2+})(M^{4+}, M^{3+})_8O_{16}$, where A^{+} = K^{+}, Na^{+}; A^{2+} = Pb^{2+}, Ba^{2+}, Sr^{2+}; M^{4+} = Mn^{4+}, Ti^{4+}; M^{3+} = Mn^{3+}, Fe^{3+}, Cr^{3+}, V^{3+}, Al^{3+}. Tunnels are built by octahedral *M*-cations and host *A*-cations and, in some cases, H_2O molecules. Actually, the content of tunnel cations can be more than 1 *pfu*. The presence of substantial amounts of bivalent octahedral cations in Mn^{4+}-dominant hollandite-type compounds is questionable (see Pasero 2005). The ideal topological symmetry of hollandite-supergroup minerals is rutile-like and tetragonal, but some samples show monoclinic distortion (Post and Bish 1989; Post et al. 1982; Meisser et al. 1999; Gatehouse et al. 1986). According to the current nomenclature of hollandite-supergroup minerals (Biagioni et al. 2013), each combination of dominant *A*-, M^{4+}- and the main charge-balancing lower-valence *M*-cation corresponds to a distinct mineral species. Depending on the dominant tetravalent cation, the hollandite supergroup is divided into the coronadite group (M^{4+}= Mn^{4+}) and the priderite group (M^{4+}= Ti^{4+}).

Owing to their microporous structures (Pasero 2005), tunnel oxides possess specific properties. In particular, some synthetic analogues of hollandite-supergroup minerals are known as materials with good charge–discharge, as well as antiferromagnetic and semiconductor properties (Strobel et al. 1984; Kijima et al. 2014). Compounds with hollandite-type structures, including synthetic analogues of hollandite-type minerals, are considered as potential matrices for the immobilization of toxic metals or radioactive isotopes, especially Cs, its daughter product Ba and related Rb- and Sr-radionuclides (Kesson 1983; Buykx et al. 1988; Aubin-Chevaldonnet et al. 2009; Costa et al. 2013; Amoroso et al. 2015; Xu et al. 2015). It was also shown that NH_3 molecules can be inserted in tunnels of a synthetic hollandite-type manganese oxide (Wang et al. 2001).

A new hollandite-supergroup mineral ferricoronadite with the idealized formula $Pb(Mn_6^{4+}Fe_2^{3+})O_{16}$ was discovered in the orogenetic zone related to the "Mixed Series" metamorphic complex situated in the Pelagonian massif near the Nežilovo village, about 40 km SW of the town of Veles, Republic of Macedonia (41°34′N, 21°34′E). A specific feature of this zone is the concentration of chalcophile elements (S, As, Sb, Zn, Pb) mainly in oxides and oxysalts, whereas sulfides and sulfosalts are present only in trace amounts (Chukanov et al. 2015). The mineral and its name have been approved by the IMA Commission on New Minerals, Nomenclature and Classification (IMA No. 2015-093).

Fig. 1 A vein enriched in ferricoronadite (middle part of the specimen with strong submetallic luster) crossing a host rock mainly consisting of zinc spinels (*black*, dull). The *white* mineral (*right*) is baryte. Field width 4 cm

The new mineral was collected in the Babuna River valley, in talus at the bottom of the Kalugeri Hill. It is the major component of hydrothermal veins up to 8 mm thick crossing a rock mainly consisting of zinc spinels (Fig. 1). The minor components of the hydrothermal veins are franklinite (relics of an earlier paragenesis), gahnite, quartz, roméite, almeidaite and zincohögbomite analogue with Fe^{3+} > Al.

The host rock enriched in zinc spinels has metasomatic origin and is confined to dolomitic marbles (see Barić 1960; Barić and Ivanov 1960). It is mainly composed by franklinite (partly replaced by gahnite) and hetaerolite and contains xenoliths of a baryte rock and accessory zincochromite, zircon, fluorapatite, Zn-bearing talc and roméite-group minerals with variable Ca/Pb, Sb/Ti and F/OH ratios.

Ferricoronadite is named in accordance with the accepted hollandite-supergroup nomenclature (Biagioni et al. 2013), as an analogue of coronadite $Pb(Mn_6^{4+}Mn_2^{3+})O_{16}$ with the major charge-compensating octahedral cation Fe^{3+} instead of Mn^{3+}.

Fragments of the holotype specimen of ferricoronadite are deposited in the collections of the Fersman Mineralogical Museum of the Russian Academy of Sciences, Moscow, Russia, registration number 4787/1, and of the National Institution Macedonian Museum of Natural History, Skopje, Republic of Macedonia, registration number PNMG 790.

Physical properties

General appearance and mechanical properties

Ferricoronadite forms aggregates of anhedral grains up to 0.6 mm across. The mineral is opaque, its color is black, and the streak is brownish black. The luster is strong submetallic to metallic. The new mineral is brittle. Hardness measured by micro-indentation (Vickers hardness number at load of 150 g) ranges from 754 to 858 kg/mm^2; mean value of 819 kg/mm^2 corresponds to Mohs' hardness ca. 6. Distinct cleavage is observed on (100). Density calculated from the empirical formula is equal to 5.538 g/cm^3.

Reflectance spectroscopy in the visible range

In reflected light ferricoronadite is anisotropic (Figs. 2, 3), light gray, without internal reflections. Reflectance values (R_{max}/R_{min}) for ferricoronadite have been measured in air using a MSF-21 microspectrophotometer (LOMO, Russia). SiC (Reflexionsstandard 474251, No. 545, Germany) was used as a standard. The reflectance values (R_{max}/R_{min}) are given in Table 1.

Infrared absorption spectroscopy

In order to obtain infrared (IR) absorption spectrum, ferricoronadite powder was mixed with anhydrous KBr, pelletized and analyzed using an ALPHA FTIR spectrometer (Bruker Optics) with the resolution of 4 cm^{-1}; 16 scans were obtained. The IR spectrum of analogous pellet of pure KBr was used as a reference.

The IR spectrum of ferricoronadite is quite similar to IR spectra of other coronadite-group minerals (Fig. 4). All bands in the range 360–700 cm^{-1} correspond to vibrations of the octahedral pseudo-framework (i.e., 3D structure based on both edge- and vertice-sharing octahedra). Weak band at 1078 cm^{-1} is assigned to a combination mode. According to Potter and Rossman (1979), major band position in IR spectra of Mn^{4+}-oxides correlates with the number of edges shared per MnO_6 octahedron, n_{edg}. In manganese hollandite-supergroup minerals, $n_{edg} = 4$ and the expected major band position is close to 500 cm^{-1}. The bands at 665 and 700 cm^{-1} may be related to vibrations involving the shortest bond *M*–O1 (see below).

Bands of O–H-stretching vibrations (in the range 2000–4000 cm^{-1}) are absent in the IR spectrum of ferricoronadite.

^{57}Fe Mössbauer spectroscopy

The Mössbauer spectra were measured on an MS1104Em spectrometer of electromechanical-type operating in the constant acceleration mode with a triangular form of the variation of the Doppler velocity of the source with respect to the absorber. ^{57}Co nuclei in the Rh matrix served as a source. The Mössbauer spectrometer was calibrated using a standard α-Fe absorber. The measurements were performed in transmission geometry at room temperature.

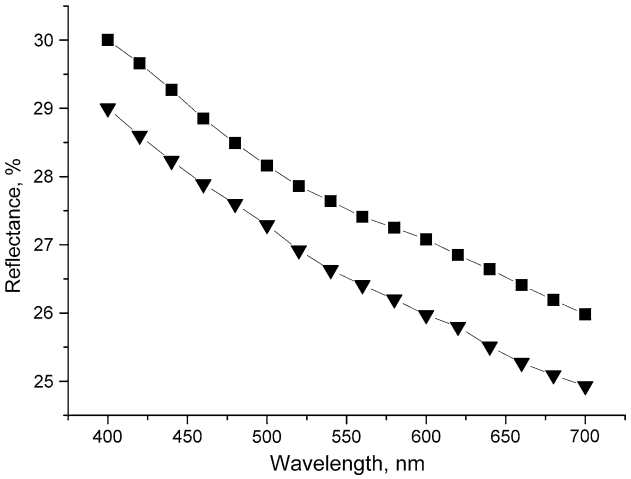

Fig. 2 Reflectance spectra of ferricoronadite (R_{max}/R_{min})

The Mössbauer spectrum of ferricoronadite is an asymmetric quadrupole doublet corresponding to Fe^{3+} (Fig. 5a). Attempts to fit this spectrum with one quadrupole doublet with resonance lines of varying intensities and widths were unsuccessful. Consequently, the asymmetry of the spectrum could not be explained by textural effects. Moreover, despite the distinct (100) cleavage of the mineral, particles of its powder are almost isometric.

Taking into account that local environment of Fe^{3+} in ferricoronadite is inhomogeneous, we restored the distribution of the hyperfine parameters using the software SpectrRelax (Matsnev and Rusakov 2012), see Fig. 5b. The reconstruction of the distribution was carried out under the assumption of linear correlation between the isomer shift (IS) and quadrupole splitting (QS). Table 1 shows parameters of the isomer shift and quadrupole splitting distribution for the Mössbauer spectrum of ferricoronadite: the maximum (max) and average (aver) values of the isomer shift and quadrupole splitting, as well as the linear correlation coefficient for them (ΔIS/ΔQS). The values of hyperfine parameters for ferricoronadite correspond to Fe^{3+} in octahedral oxygen coordination.

Mn *K*-edge XANES spectroscopy

Mn *K*-edge XANES spectroscopy has been applied to determine mean Mn valence in ferricoronadite. Ferricoronadite and reference samples were analyzed by using XANES (X-ray absorption near edge structure) spectroscopy at the

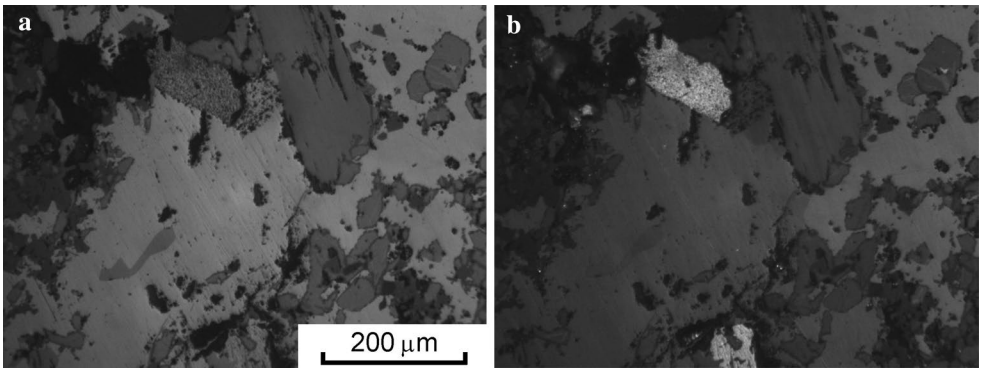

Fig. 3 **a** A fragment of polished section of polymineral aggregate containing ferricoronadite in reflected unpolarized light (ferricoronadite is *light gray*) and **b** image of the same fragment obtained with an analyzer and demonstrating distinct anisotropy of the new mineral

Table 1 Parameters of the isomer shift and quadrupole splitting distribution for the Mössbauer spectrum of ferricoronadite

IS_{max} (mm/s)	QS_{max} (mm/s)	IS_{aver} (mm/s)	QS_{aver} (mm/s)	ΔIS/ΔQS
0.342(7)	0.486(18)	0.336(2)	0.564(5)	−0.079(14)

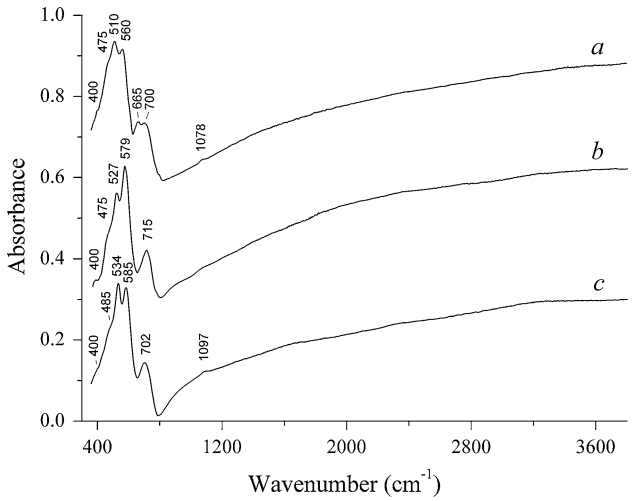

Fig. 4 Powder IR absorption spectra of coronadite-group minerals: (*a*) ferricoronadite (*b*) coronadite $Pb_{1.00}(Mn_{7.58}Al_{0.15}V_{0.14}Fe_{0.07}Mg_{0.06})O_{16}$ from the Imiter mine, Morocco, and (*c*) cryptomelane $(K_{0.6}Na_{0.15}Ba_{0.05})(Mn_{7.9}Al_{0.1})O_{16}$ from the Kent granite massif, Central Kazakhstan

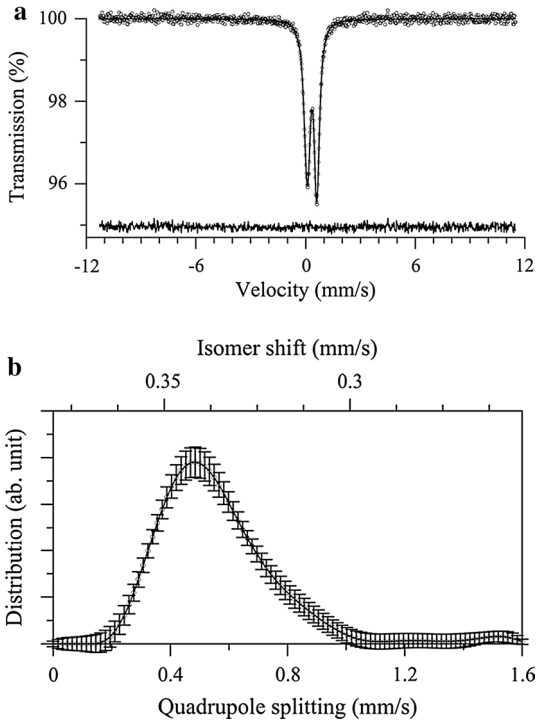

Fig. 5 Mössbauer spectrum (**a**) and hyperfine parameters distribution (**b**) for ^{57}Fe in ferricoronadite

Mn *K*-edge on powdered minerals pressed to pellets (7 mm diameter). XANES spectra were collected at the SUL-X beamline (Wiggler as radiation source) of the ANKA synchrotron radiation facility (Angströmquelle Karslruhe Institute of Technology (KIT), Germany). The electron storage ring operation conditions were 2.5 GeV and the electron current varied from about 150–90 mA during a 13-h beamtime shift. A Si(311) monochromator crystal pair was used providing a better energy resolution than with Si(111) crystal pairs which is required to distinguish spectral features, especially in the pre-edge range XANES spectra. A focused beam of about 0.15 mm (hor.) and 0.1 mm (vert.) was used (slit 4 opening 0.3 mm × 0.3 mm). Further improvement of the energy resolution has been achieved by setting the vertical opening of slit 3 to 0.5 mm.

XANES spectrum of a Mn metal foil was measured together with those of mineral samples for the energy calibration of the monochromator. The inflection point of the

Table 2 Reflectance values for ferricoronadite

λ (nm)	R_{max}	R_{min}
400	30.0	29.0
420	29.7	28.6
440	29.3	28.2
460	28.9	27.9
470	**28.7**	**27.8**
480	28.5	27.6
500	28.2	27.3
520	27.9	26.9
540	27.6	26.6
546	**27.6**	**26.6**
560	27.4	26.4
580	27.3	26.2
589	**27.2**	**26.1**
600	27.1	26.0
620	26.9	25.8
640	26.6	25.5
650	**26.5**	**25.4**
660	26.4	25.3
680	26.2	25.1
700	26.0	24.9

Reflectance values for four standard wavelengths are given in bold type

Mn *K*-edge was set to 6539 eV. All spectra were collected in the transmission mode using three ionization chambers (ADC) in the energy range 6419–6920 eV. For the pre-edge background, energy steps of 5 eV were chosen between −120 and −50 eV, 2 eV between −50 and −4 eV, for the pre-edge 0.15 eV between −4 and 6 eV with four times increased measuring time and for the edge 0.25 eV between 6 and 30 eV related to the chosen E_0 of 6539 eV. At least, three spectra were collected for each sample and averaged for further data processing. Pre-edge and post-edge background was fitted by a polynomial and subtracted. The normalization on atomic absorption was based on the average absorption coefficient of the spectral region after the edge and set to 1 (Table 2).

The low energy flank of the spectrum of ferricoronadite is close to the flank for Mn(IV) reference (pyrolusite), but shows somewhat enhanced absorption in the range 6549–6559 eV corresponding to Mn(III) (Fig. 6). Taking into account the XANES data, as well as highly oxidizing conditions of mineral formation (Chukanov et al. 2015), it can be assumed that additional (subordinate) lower-valence state of manganese is Mn^{3+}. Moreover, it is accepted today that the reduced state of Mn in all minerals of the hollandite supergroup is Mn^{3+} and not Mn^{2+} (see Post and Bish 1989; Meisser et al. 1999; Pasero 2005; Biagioni et al. 2013). However, the presence of a weak absorption maximum at

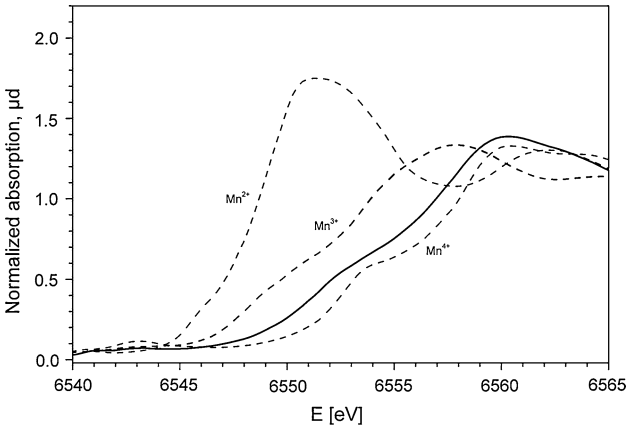

Fig. 6 Mn *K*-edge XANES spectrum of ferricoronadite (*solid line*). The spectra of rhodochrosite $MnCO_3$ (Mn^{2+}), bixbyite Mn_2O_3 (Mn^{3+}) and pyrolusite MnO_2 (Mn^{4+}) are given for comparison by *dashed lines*

6552 eV in the difference spectrum "ferricoronadite minus pyrolusite" (Fig. 7) indicates that trace amounts of Mn^{2+} cannot be excluded.

Chemical composition

Five chemical analyses were carried out using a digital scanning electron microscope Tescan VEGA-II XMU equipped by an Oxford INCA Wave 700 spectrometer (WDS mode, accelerating voltage of 20 kV, electron beam current of 20 nA, beam diameter of 3 μm and counting times of 100 s for each element). Calculations of results of the X-ray microanalysis were carried out by means of the INCA Energy 300 software package. Analytical data are given in Table 3. Contents of other elements with atomic numbers >8 are below their detection limits. H_2O was not analyzed because of the absence of bands corresponding to O–H vibrations in the IR spectrum (see above).

The empirical formula (based on 8 cations Mn + Fe + Ti + Al + Zn *pfu* and the Mn^{3+}/Mn^{4+} ratio calculated from charge balance) is $Pb_{1.03}Ba_{0.32}(Mn^{4+}_{4.85}Fe^{3+}_{1.35}Mn^{3+}_{1.18}Ti_{0.49}Al_{0.09}Zn_{0.04})_{\Sigma 8.00}O_{16}$. The simplified formula could be written as follows: $PbBa_x[Mn^{4+}_{6-x}(Fe^{3+}, Mn^{3+})_{2+x}]O_{16}$. The idealized (end-member) formula $Pb(Mn_6{}^{4+}Fe_2{}^{3+})O_{16}$ requires PbO 24.67, Fe_2O_3 17.66, MnO_2 57.67, total 100.00 wt%.

X-ray diffraction data and crystal structure

Powder X-ray diffraction data were collected with a Rigaku R-AXIS Rapid II single-crystal diffractometer equipped with cylindrical image plate detector using Debye-Sherrer

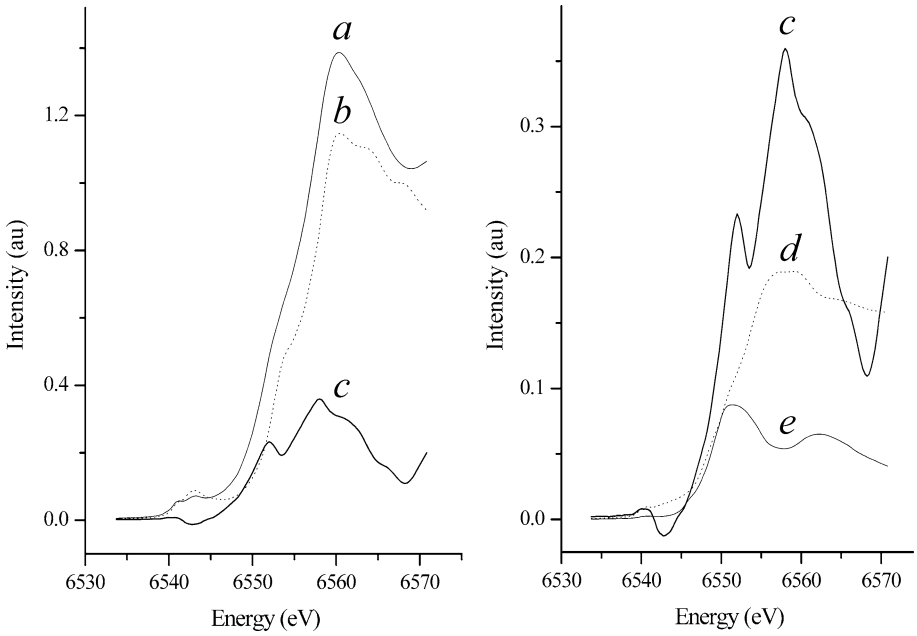

Fig. 7 *Left* Mn *K*-edge XANES spectra of ferricoronadite (*a*), pyrolusite (*b*) and their difference (*c*). *Right* comparison of the difference Mn *K*-edge XANES spectrum (ferricoronadite minus pyrolusite) with the spectra of bixbyite (*d*) and rhodochrosite (*e*). The spectra *d* and *e* are rescaled for convenience

Table 3 Chemical composition (in wt%) for ferricoronadite

Constituent	Mean	Range	Standard deviation	Probe Standard
BaO	5.16	4.56–5.870.47		$BaSO_4$
PbO	24.50	23.42–25.680.80		PbTe
ZnO	0.33	0–0.610.27		Zn
Al_2O_3	0.50	0.42–0.700.11		Albite
Fe_2O_3	11.45	11.01–11.930.33		Fe_2O_3
TiO_2	4.19	3.64–4.460.30		$MnTiO_3$
MnO_2	44.81	54.85–56.62[a]0.65[a]		$MnTiO_3$
Mn_2O_3	9.90			
Total	100.84			

Total Mn determined as 55.71 wt% MnO_2 was divided into Mn_2O_3 and MnO_2 based on charge-balance requirements

[a] For total manganese considered as MnO_2

geometry ($d = 127.4$ mm). Data (in Å for Co*K*α) are given in Table 4.

The obtained diffraction pattern was indexed in the tetragonal (space group *I*4/*m*) unit cell, in agreement with the single-crystal diffraction data. Unit-cell parameters refined from the powder data are: $a = 9.9073(9)$, $c = 2.9023(4)$ Å, $V = 284.87(9)$ Å^3.

The single-crystal X-ray data were collected at room temperature by means of a Bruker SMART APEX2 diffractometer (Bruker 2009) with graphite monochromatized Mo*K*α radiation ($\lambda = 0.71073$ Å) and a CCD detector using the $\omega - \theta$ scanning mode. Raw data were integrated using the program SAINT and scaled, merged and corrected for Lorentz-polarization effects using the SADABS package. A total of 1899 reflections within the sphere limited by $\theta = 30.73°$ were measured. The experimental details of the data collection and refinement results are listed in Table 5. The structure determination and refinement were carried out using the JANA2006 program package (Petříček et al. 2006). Illustrations were produced with the JANA2006 program package in combination with the program DIAMOND (Brandenburg and Putz 2005).

The ideal topological symmetry of 2 × 2 tunnel oxides is tetragonal (space group *I*4/*m*), but different kinds of cation ordering and framework distortions may lower symmetry from tetragonal to monoclinic (space group *I*2/*m*, $P2_1/n$ or *P*2/*m*). Moreover, different arrangements of extra-framework cations cause aperiodic commensurate/incommensurate modulated structures and superstructures of hollandite-like compounds (Bolotina et al. 1992; Biagioni et al. 2013). The space group *I*4/*m* was chosen for ferricoronadite based on the analysis of systematic absences of reflections. Atomic scattering factors for neutral atoms together with anomalous dispersion corrections were taken from *International Tables for X-Ray Crystallography* (Ibers and Hamilton 1974). The initial model for the ferricoronadite structure refinement was based on the atom coordinates for "ankangite" $Ba(Ti, V^{3+})_8O_{16}$ (Biagioni et al. 2009). It is to be noted that according to the current nomenclature ankangite is renamed into mannardite.

The final refinement cycles converged with $R_1 = 2.60$, $wR_2 = 4.06$ and GooF = 0.98 for 242 independent reflections with $I > 2\sigma(I)$. The highest peak and the deepest hole in the final residual electron density map are 0.81 and −0.43 e Å^{-3}, respectively. Table 6 shows the fractional atomic coordinates, occupancy, site symmetry, equivalent

Table 4 Powder X-ray diffraction data (d in Å) for ferricoronadite

I_{obs} (%)	d_{obs} (Å)	I_{calc} (%)[a]	d_{calc} (Å)[b]	hkl
10	6.98	6	7.003	110
33	3.497	39	3.502	220
100	3.128	58, 100	3.132, 3.132	−130, 130
3	2.781	2	2.782	011
3	2.469	1	2.476	040
27	2.424	21, 28	2.425, 2.425	−121, 121
23	2.214	20, 12	2.215, 2.215	240, −240
17	2.178	21	2.178	031
3	1.994	4	1.994	−231
8	1.942	10	1.942	−150
15	1.850	9, 17	1.850, 1.850	141, −141
6	1.750	8	1.751	440
5	1.699	3, 6	1.699, 1.699	−350, 350
16	1.651	28	1.651	060
5	1.564	1	1.566	260
18	1.554	9, 21	1.553, 1.553	−251, 251
3	1.450	4	1.449	002
4	1.420	5	1.419	112
2	1.401	1, 2	1.401, 1.401	−170, 550
4	1.392	7	1.391	022
14	1.365	18, 3	1.365, 1.365	−451, 451
6	1.301	8, 6	1.301, 1.301	−370, 370
3	1.253	8	1.251	042
3	1.232	1, 1, 6	1.232, 1.232, 1.231	−271, 271, 332
3	1.168	7	1.167	660
2	1.163	1, 4	1.162, 1.162	−561, 152
4	1.131	1, 2, 1, 1	1.131, 1.131, 1.131, 1.131	181, −181, 471, −471
2	1.108	3, 1	1.107, 1.107	−480, 480
4	1.094	2, 8	1.094, 1.094	−190, 190
3	1.090	4	1.089	062
2	1.065	2, 5	1.064, 1.064	262, 2–62

[a] For the calculated pattern, only reflections with intensities ≥1 are given

[b] For the unit-cell parameters calculated from single-crystal data

atomic displacement parameters and bond-valence sums. Anisotropic atomic displacement parameters are presented in Table 7.

Discussion

Based on the refined site-scattering factors, the crystal-chemical formula of ferricoronadite is (Z = 1): $^{A1}(Ba_{0.32}Pb_{0.13})$ $^{A2}Pb_{0.90}$ $^{M}(Mn^{4+}_{4.85}Fe^{3+}_{1.35}Mn^{3+}_{1.18}Ti_{0.49}Al_{0.09}Zn_{0.04})O_{16}$. The structure of ferricoronadite is similar to that of other members of the coronadite group belonging to the hollandite supergroup (Miura 1986; Biagioni et al. 2009, 2013) and is based on double chains of edge-shared M-octahedra running along c. These chains share corners with neighboring double chains to form a pseudo-framework structure containing large 2 × 2 tunnels (Pasero 2005; see Fig. 8). The effective tunnel width calculated according to McCusker et al. (2003) by subtracting the ionic diameter of O^{2-} (2.7 Å) from the shortest O···O distances across the tunnel is ~3.3 × 3.3 Å. According to the recommendations of the International Zeolite Association (Liebau 2003; McCusker 2005), the crystal-chemical formula of ferricoronadite can be written as follows (Z = 1): $\left|(Pb_{1.03}Ba_{0.32})^{[12]}\right|\left[\left(Mn^{4+}_{4.85}Fe^{3+}_{1.35}Mn^{3+}_{1.18}Ti_{0.49}Al_{0.09}Zn_{0.04}\right)^{[6]}O_{16}\right]h\{3\}_p\{1^{\|}[001](8\text{-ring})\}(I4/m)$, indicating that (1) the guests are Pb^{2+} and Ba^{2+} ions and (2) 3D host structure consists of one-dimensional channel system with an eight-membered ring pore opening along the [001] direction.

Octahedral site

In ferricoronadite, there is only one independent octahedral M-site, which is predominantly occupied by Mn^{4+} with admixtures of Fe^{3+}, Mn^{3+} and Ti. The average M–O distance is 1.933 Å ($V^{(M)}$ = 9.47 Å^3). The analysis of geometrical characteristics indicates the high degree of octahedral distortion $\Delta^{(M)} = 0.25$, where $\Delta = (1/6)\sum_{i=1-6}\{[(M\text{–O})_i - \langle M\text{–O}\rangle]/\langle M\text{–O}\rangle\}^2 \times 10^3$ (Brown and Shannon 1973), as well as quadratic elongation $\lambda^{(M)}_{oct} = 1.01$, where $\lambda_{oct} = (1/6)\sum_{i=1-6}(l_i/l_o)^2$ (Robinson et al. 1971). These characteristics confirm the occupancy of the M-site by heterovalent ions (Fig. 9).

Tunnel site

In the structure of ferricoronadite, the A-site situated in the 2 × 2 tunnel is split into the subsites $A1$- and $A2$ with the $A1$–$A2$ distance of 0.70 Å (Fig. 10). The subsite $A1$ is occupied predominantly by Ba^{2+} with admixture of Pb^{2+} and has 12-fold coordination with the average distance $\langle A1\text{–O}\rangle$ = 3.044 Å (Fig. 11a). The subsite $A2$ contains only Pb^{2+} and is located in the same 12-fold polyhedron (with $\langle A1\text{–O}\rangle$ = 3.111 Å), but is shifted from its center (Fig. 11b). In this reference, it is to be noted that the role of the $6s^2$ lone pair in distorting the coordination polyhedron of Pb^{2+} has been discussed in numerous publications (see, e.g., Moore 1988; Larrégola et al. 2010; Dörsam et al. 2011).

The unit-cell translation along the tunnel (c ~ 2.90 Å) is shorter than the minimum Ba^{2+}–Ba^{2+}/Ba^{2+}–Pb^{2+}/

Table 5 Crystal parameters, data collection and structure refinement details for ferricoronadite

Crystal data	
Formula	$PbBa_x[Mn^{4+}_{6-x}(Fe^{3+}, Mn^{3+})_{2+x}]O_{16}$
Formula weight (g)	948.5
Temperature (K)	293
Cell setting	Tetragonal
Space group	*I*4/*m*
a (Å)	9.9043(7)
c (Å)	2.8986(9)
V (Å^3)	284.34(9)
Z	1
Calculated density, D_x (g cm^{-3})	5.539
Crystal size (mm)	0.11 × 0.12 × 0.15
Crystal form	Anhedral grain
Data collection	
Diffractometer	SMART APEX2 CCD
Radiation (λ)	MoK_α; 0.71073
Absorption coefficient [μ (mm^{-1})]	24.919
F (000)	429
Data range [θ (°)]; *h*, *k*, *l*	2.91–30.73; $-14 < h < 13$, $-14 < k < 14$, $-4 < l < 4$
No. of measured reflections	1899
Total reflections (N_2)/unique(N_1)	258/242
Criterion for observed reflections	$I > 2\sigma(I)$
R_{int} (%)	3.95
Refinement	
Refinement on	Full-matrix least squares on *F*
Weight scheme	$1/(\sigma^2\|F\| + 0.001225\ F^2)$
R_1, wR_2	2.60, 4.06
GooF	0.98
Max./min. residual *e* density (e Å^{-3})	0.81/−0.43

$R_1 = \sum||F_{obs}| - |F_{calc}||/\sum|F_{obs}|$; $wR_2 = \{\sum[w(F^2_{obs} - F^2_{calc})^2]/\sum[w(F^2_{obs})^2]\}^{1/2}$; GooF $= \{\sum[w(F^2_{obs} - F^2_{calc})]/(n-p)\}^{1/2}$ where *n* is a number of reflections and *p* is a number of refined parameters

Table 6 Fractional coordinates, site multiplicities (*Q*), equivalent displacement parameters of atoms (U_{eq}, Å^2), and bond-valence sum (BVS, v.u.) in the structure of ferricoronadite

Site	*x*	*y*	*z*	*Q*	U_{eq}	BVS
*A*1	0.5	0.5	0.5	2*a*	0.037(1)	0.36
*A*2	0.5	0.5	0.259(2)	4*e*	0.0356(5)	0.32
M	0.1653(1)	0.6502(1)	0.5	8 *h*	0.0047(2)	3.73
O1	0.1665(3)	0.4585(3)	0.5	8 *h*	0.0077(7)	2.06
O2	0.2979(3)	0.6536(3)	0	8 *h*	0.0080(7)	1.92

U_{eq} is defined as one-third of the trace of the orthogonalized U_{ij} tensor. Bond-valence sum calculations were performed using the bond-length parameters from Brown and Altermatt (1985) and Krivovichev and Brown (2001) (for Pb^{2+}). In mixed sites, bond-valence contribution of each cation has been weighted according to its occupancy

Pb^{2+}–Pb^{2+} distances corresponding to *A*1–*A*1, *A*1–*A*2 and *A*2–*A*2 distances of adjacent unit cells along *c*, which are acceptable from the standpoint of electrostatic repulsion. Therefore, partial occupancy of these sites is required, which leads to different local sequences of *A*-sites (Fig. 12).

Among hollandite-related minerals, the highest contents of ferric iron are known in ferrihollandite (up to 12.63 wt% Fe_2O_3 in a sample from Stuor Njvoskes, Sweden—see Ödman 1950) and in priderite from the West Kimberley area, Western Australia (12.4 wt%—Norrish 1951). In most

Table 7 Anisotropic atomic displacement parameters for ferricoronadite

Site	U^{11}	U^{22}	U^{33}	U^{12}	U^{13}	U^{23}
*A*1	0.038(1)	0.038(1)	0.033(3)	0	0	0
*A*2	0.039(1)	0.039(1)	0.029(1)	0	0	0
M	0.006(1)	0.006(1)	0.003(1)	−0.001(1)	0	0
O1	0.014(1)	0.005(1)	0.004(1)	0.001(1)	0	0
O2	0.009(1)	0.008(1)	0.008(1)	−0.001(1)	0	0

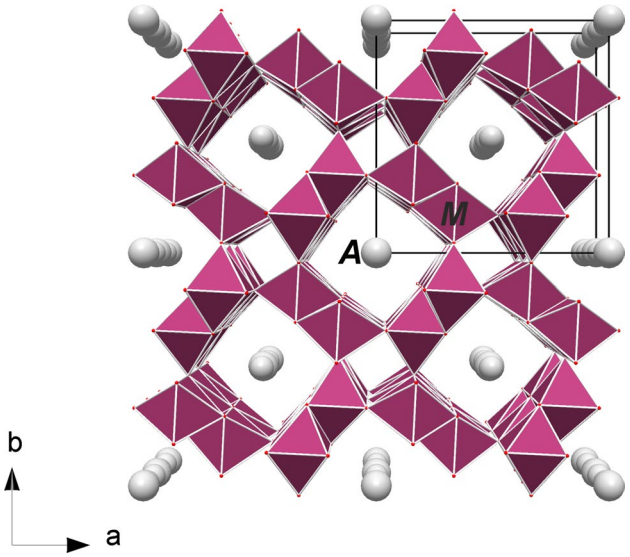

Fig. 8 Crystal structure of ferricoronadite: general view. The unit cell is outlined

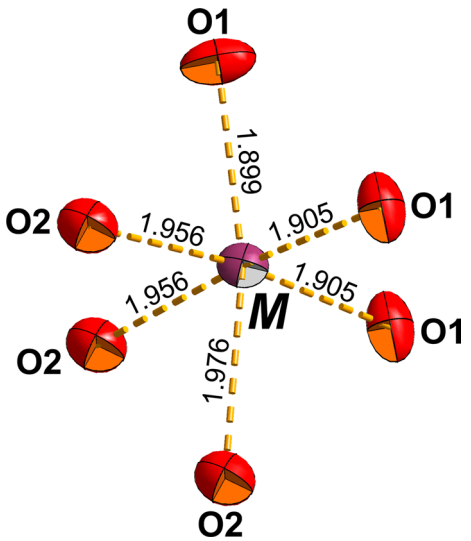

Fig. 9 Octahedron MO_6 in ferricoronadite

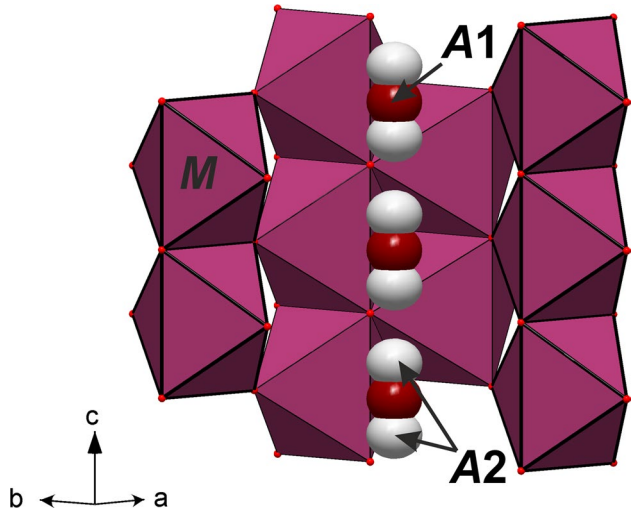

Fig. 10 Arrangement and splitting of the *A*-sites in the ferricoronadite structure

cases, coronadite is the product of supergene processes. In supergene coronadite, the content of Fe_2O_3 rarely exceeds 2 wt%. The occurrence of hypogenic ferricoronadite in the orogenetic zone of the Pelagonian massif is unique.

As it is noted above, it is widely accepted today that the reduced state of Mn in all minerals of the hollandite supergroup is Mn^{3+} and not Mn^{2+}. Numerous data show that the presence of Fe^{2+} as the main charge-balancing cation is also questionable. According to Mössbauer data, in ferricoronadite all iron is trivalent. Investigations of synthetic iron-bearing hollandite-type compounds with nominal compositions of $K_2Fe_2Ti_6O_{16}$ and $BaFe_2Ti_6O_{16}$ and one natural sample of priderite by means of Mössbauer spectroscopy show that all iron is octahedral Fe^{3+} with no evidence for Fe^{2+} (McCammon et al. 1999). In synthetic Fe-doped cryptomelanes, iron is also present as Fe^{3+} (Yin et al. 2015).

Comparative data for ferricoronadite and some related minerals are given in Table 8.

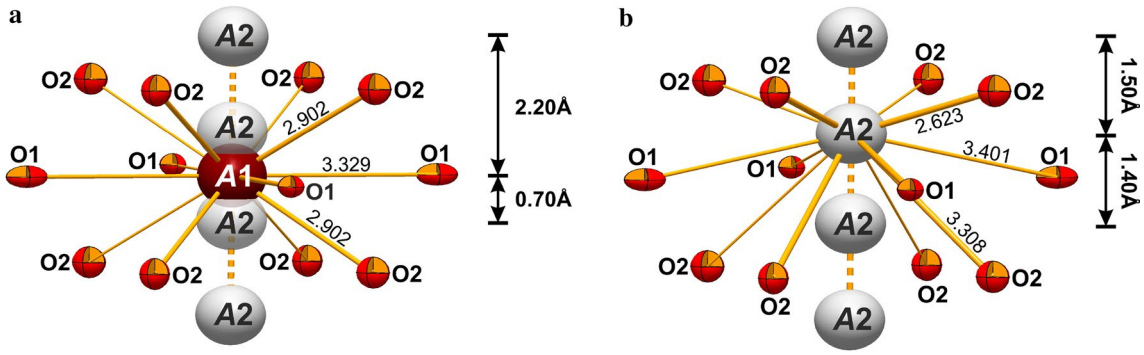

Fig. 11 Local environments of the sites *A*1 (**a**) and *A*2 (**b**)

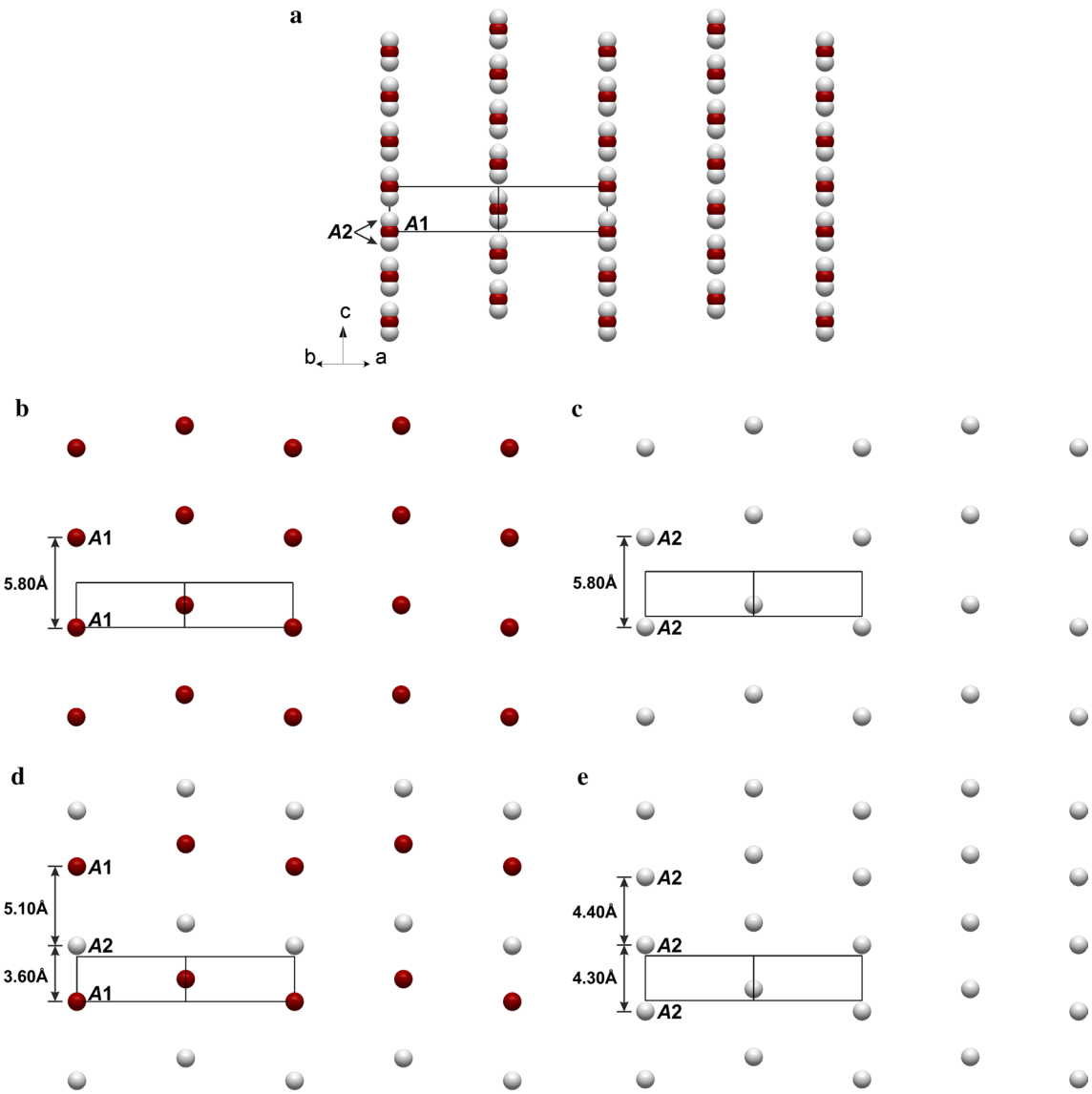

Fig. 12 Statistical distribution of tunnel cations (**a**) and their possible arrangements (**b**–**e**) in the structure of ferricoronadite. All figures are given for the (110)-plane projection

Table 8 Comparative data for ferricoronadite and closely related hollandite-supergroup minerals

Mineral	Ferricoronadite	Coronadite	Ferrihollandite
End-member formula	$Pb(Mn_6^{4+}Fe_2^{3+})O_{16}$	$Pb(Mn_6^{4+}Mn_2^{3+})O_{16}$	$Ba(Mn_6^{4+}Fe_2^{3+})O_{16}$
Crystal system	Tetragonal	Monoclinic	Monoclinic
Space group	*I*4/*m*	*I*2/*m*	*P*2/*n*
a (Å)	9.9043	9.913–9.938	10.0001
b (Å)	9.9043	2.865–2.868	5.7465
c (Å)	2.8986	9.834–9.843	9.8076
β (°)	90	90.20–90.39	90.713
V (Å^3)	284.34	280.26–280.28	563.56
Z	1	1	2
Strong lines of the powder X-ray diffraction pattern: *d*, Å (*I*, %)	3.497 (39)	3.466 (60)	7.046 (93)[a]
	3.128 (100)	3.104 (100)	6.958 (94)[a]
	2.424 (27)	2.400 (40)	5.000 (84)[a]
	2.214 (23)	2.205 (40)	4.903 (100)[a]
	2.178 (17)	2.155 (20)	3.144 (99)[a]
	1.850 (15)	1.836 (20)	3.119 (99)[a]
	1.651 (16)	1.542 (50)	2.411 (66)[a]
	1.554 (18)		2.403 (56)[a]
Density (g cm^{-3})	5.538 (calc.)	5.246–5.505 (meas.) 5.45 (calc.)	4.92 (calc.)
Sources	This work	Frondel and Heinrich (1942), Perseil and Pinet (1976), Post and Bish (1989)	Biagioni et al. 2014

[a] Calculated from the structural data (Biagioni et al. 2014); measured powder X-ray diffraction data of ferrihollandite were not reported by Biagioni et al. (2014)

Acknowledgments This work was financially supported by the Russian Foundation for Basic Research (Grants Nos. 14-05-00276-a, 16-35-60101-mol-a-dk and 16-03-00691a).

References

Amoroso J, Marra J, Conradson SD, Tang M, Brinkman K (2015) Melt processed single phase hollandite waste forms for nuclear waste immobilization: $Ba_{1.0}Cs_{0.3}A_{2.3}Ti_{5.7}O_{16}$; A = Cr, Fe, Al. J Alloys Compds 584:590–599

Aubin-Chevaldonnet V, Caurant D, Gourier D, Charpentier T, Esnouf S (2009) Synthesis and stability under electron irradiation of a hollandite structure-type $Ba_{1.16}Al_{2.32}Ti_{5.68}O_{16}$ ceramic envisaged for radioactive cesium immobilization. C R Chim 12:1079–1092

Barić Lj (1960) Piemontit, gahnit und rutil aus dem Fundort der Blei und Zincerze bei dem Dorfe Nezilovo in Mazedonien. Glasnik Prirodnjackogo Muzeja Beograd Ser A 13:200–204

Barić Lj, Ivanov T (1960) Mineralvergesellschaftung in der Umgebung des Dorfes Nežilovo am Jakupica-Gebirge in Mazedonien. Bull Sci (Zagreb) 5:2

Biagioni C, Orlandi P, Pasero M (2009) Ankangite from the Monte Arsiccio mine (Apuan Alps, Tuscany, Italy): occurrence, crystal structure, and classification problems in cryptomelane group minerals. Period Mineral 78:3–11

Biagioni C, Capalbo C, Pasero M (2013) Nomenclature tunings in the hollandite supergroup. Eur J Mineral 25:85–90

Biagioni C, Capalbo C, Lezzerini M, Pasero M (2014) Ferrihollandite, $BaMn_6^{4+}Fe_2^{3+}O_{16}$, from Apuan Alps, Tuscany, Italy: description and crystal structure. Eur J Mineral 26:171–178

Bolotina N, Dmitrieva MT, Rastsvetaeva RK (1992) Modulated structures of a new natural representative of the hollandite series. Sov Phys Crystallogr 37:311–315

Brandenburg K, Putz H (2005) *DIAMOND* version 3. Crystal Impact GbR, Bonn

Brown ID, Altermatt D (1985) Bond-valence parameters obtained from a systematic analysis of the inorganic crystal structure database. Acta Cryst B 41:244–247

Brown ID, Shannon RD (1973) Empirical bond strength—bond lengths curves for oxides. Acta Cryst A 29:266–282

Bruker (2009) APEX2 and SAINT. Bruker AXS Inc, Madison, Wisconsin, USA

Buykx WL, Hawkins K, Levins DM, Mitamura H, Smart RS, Stevens GT, Watson KG, Weedon D, White TJ (1988) Titanate ceramics for the immobilization of sodium-bearing high-level nuclear waste. J Am Ceram Soc 71(8):678–688

Chukanov NV, Jančev S, Pekov IV (2015) The association of oxygen-bearing minerals of chalcophile elements in the orogenetic zone related to the "Mixed Series" complex near Nežilovo, Republic of Macedonia. Maced J Chem Chem Eng 34(1):115–124

Costa GCC, Xu HW, Navrotsky A (2013) Thermochemistry of barium hollandites. J Am Ceram Soc 63:1554–1561

Dörsam G, Liebscher A, Wunder B, Franz G, Gottschalk M (2011) Synthesis of Pb-zoisite and Pb-lawsonite. N Jbhrb Mineral Abh 188(2):99–110

Frondel C, Heinrich EW (1942) New data on hetaerolite, hydrohetaerolite, coronadite, and hollandite. Am Mineral 27:48–56

Gatehouse BM, Jones GC, Pring A, Symes RF (1986) The chemistry and structure of redledgeite. Mineral Mag 50:709–715

Ibers JA, Hamilton WC (eds) (1974) International tables for X-ray crystallography, vol IV. The Kynoch Press, Birmingham

Kesson SE (1983) The immobilization of cesium in synrock hollandite. Radioact Waste Manag Environ Restor 4(1):53–72

Kijima N, Sakao M, Tanuma Y, Kataoka K, Igarashi K, Akimoto J (2014) Synthesis, crystal structure, and electrochemical properties of hollandite-type $K_xTi_{1-y}Mn_yO_2$. Solid State Ionics 262:14–17

Krivovichev SV, Brown ID (2001) Are the compressive effects of encapsulation an artifact of the bond valence parameters. Z Kristallogr 216:245–247

Larrégola SA, Alonso JA, Algueró M, Jiménez R, Suard E, Porcher F, Pedregosa JC (2010) Effect of the Pb^{2+} lone electron pair in the structure and properties of the double perovskites $Pb_2Sc(Ti_{0.5}Te_{0.5})O_6$ and $Pb_2Sc(Sc_{0.33}Te_{0.66})O_6$: relaxor state due to intrinsic partial disorder. Dalton Trans 39:5159–5165

Liebau F (2003) Ordered microporous and mesoporous materials with inorganic hosts: definitions of terms, formula notation and systematic classification. Microporous Mesoporous Mater 58:15–72

Matsnev ME, Rusakov VS (2012) SpectrRelax: an application for Mössbauer spectra modeling and fitting. In: Mössbauer spectroscopy in materials science: proceedings of the AIP conference, vol 1489, pp 178–185

McCammon C, Mitchell RH, Chakhmouradian AR (1999) Mössbauer spectra of priderite and synthetic iron-bearing hollandite. Can Mineral 37:991–995

McCusker L (2005) IUPAC nomenclature for ordered microporous and mesoporous materials and its application to non-zeolite microporous mineral phases. Rev Mineral Geochem 57:1–16

McCusker LB, Liebau F, Engelhardt G (2003) Nomenclature of structural and compositional characteristics of ordered microporous and mesoporous materials with inorganic hosts. Microporous Mesoporous Mater 58:3–13

Meisser N, Perseil E-A, Brugger J, Chiappero P-J (1999) Strontiomelane, $SrMn_6^{4+}Mn_2^{3+}O_{16}$, a new mineral of the cryptomelane group from St. Marcel-Praborna, Aosta Valley, Italy. Can Mineral 37:673–678

Miura H (1986) The crystal structure of hollandite. Mineral J 13:119–129

Moore PB (1988) The joesmithite enigma: note on the 6 s^2 Pb^{2+} lone pair. Am Mineral 73:843–844

Norrish K (1951) Priderite, a new mineral from the leucite-lamproites of the west Kimberley area, Western Australia. Mineral Mag 29:496–501

Ödman OH (1950) Manganese mineralization in the Ultevis district, Jokkmokk, North Sweden. Part 2: mineralogical notes. Sveriges Geologiska Undersökning Serie C 516:1–27

Pasero M (2005) A short outline of the tunnel oxides. Rev Mineral Geochem 57:291–305

Perseil EA, Pinet M (1976) Contribution à la connaissance des romanéchites et des cryptoméelanes—coronadites—hollandites. Traits essentiels et paragenèses. Contrib Mineral Petrol 55:191–204

Petříček V, Dušek M, Palatinus L (2006) Jana 2006. Structure determination software programs. Institute of Physics, Praha

Post JE, Bish DL (1989) Rietveld refinement of the coronadite structure. Am Mineral 74:913–917

Post JE, von Dreele RB, Buseck PR (1982) Symmetry and cation displacements in hollandites: structure refinements of hollandite, cryptomelane and priderite. Acta Cryst B 38:1056–1065

Potter RM, Rossman GR (1979) The tetravalent manganese oxides: identification, hydration, and structural relationships by infrared spectroscopy. Am Mineral 64:1199–1218

Robinson K, Gibbs GV, Ribbe PH (1971) Quadratic elongation: a quantitative measure of distortion in coordination polyhedra. Science 172:567–570

Strobel P, Vicat J, Qui DT (1984) Thermal and physical properties of hollandite-type $K_{1.3}Mn_8O_{16}$ and $(K, H_3O)\ xMn_8O_{16}$. J Solid State Chem 55:67–73

Wang Z-M, Tezuka S, Kanoh H (2001) Characterization of the structural and surface properties of a synthesized hydrous hollandite by gaseous molecular adsorption. Chem Mater 13:530–537

Xu H, Wu L, Zhu J, Navrotsky A (2015) Synthesis, characterization and thermochemistry of Cs-, Rb- and Sr-substituted barium aluminium titanate hollandites. J Nucl Mater 459:70–76

Yin H, Dai X, Zhu M, Li F, Feng X, Liu F (2015) Fe-doped cryptomelane synthesized by refluxing at atmosphere: structure, properties and photocatalytic degradation of phenol. J Hasard Mater 296:221–229